Drop Signal Phase Offset Independent Soft-ROADMs for Point-to-Multipoint 5G Fronthauls

Omaro Fawzi Abdelhamid Gonem
School of Computer Science and Electronic Engineering
Bangor University
Bangor, UK
o.gonem@bangor.ac.uk

Roger Philip Giddings
School of Computer Science and Electronic Engineering
Bangor University
Bangor, UK
r.p.giddings@bangor.ac.uk

Jianming Tang
School of Computer Science and Electronic Engineering
Bangor University
Bangor, UK
j.tang@bangor.ac.uk

***Abstract*— A novel MIMO-based I/Q Crosstalk Mitigation technique, is demonstrated to effectively mitigate soft-ROADM drop RF signal phase-offset and fiber-induced chromatic-dispersion effects. Thus, simplifying the practical implementation of soft-ROADM-based Point-to-Multipoint 5G fronthaul.**

Keywords*— *5G, digital filtering, digital signal processing (DSP), fronthaul, point-to-multipoint, ROADMs.

I. Introduction

Due to the immense continuous growth in the emergence of widely diverse network applications with significantly different connectivity QoS, latency, and bandwidth requirements such as on-demand video streaming, Internet-of-Things (IoT), and cloud-based applications, there is a pressing need to develop cost-effective and high-performance mobile fronthauls as vital network segments connecting radio remote heads (RRHs) and baseband units (BBUs) in cloud radio access networks (C-RANs). A future fronthaul is required to provide high peak throughput, low latency, high reliability, and highly-secure dynamic services. To sustain cost-effectiveness, highly flexible and dynamically reconfigurable point-to-multipoint (PtMP) connectivity is essential to achieve excellent network elasticity, and traffic dependent adaptability [1].

The current C-RAN fronthaul is mainly based on a bandwidth-consuming common public radio interface (CPRI), which transports digitized in-phase (I) and quadrature-phase (Q) samples at a fixed traffic-independent data rate. This leads to very stringent requirements such as huge bandwidth, low jitter and tight synchronization [2]. In addition, the fronthaul bandwidth requirement is directly proportional to the number of deployed antennas [3], this makes the adoption of C-RANs challenging for 5G networks, as it becomes extremely expensive to support highly desired advanced multi-antenna-based solutions such as massive multiple-input multiple-output (mMIMO), beamforming, milli-meter wave (mmWave), and terahertz communications.

To overcome these technical challenges, the 3rd Generation Partnership Project (3GPP) has proposed different C-RAN functional splits with less stringent fronthaul data rates and latency requirements. This has led to the realization of an enhanced CPRI (eCPRI) standard supporting a variety of functional splits between a centralized unit (CU), a distributed unit (DU) and a radio unit (RU) [4]. Unlike CPRI, eCPRI has a traffic-dependent data rate, lower latency/jitter requirements, offers a tenfold reduction in the bandwidth requirements, and allows the transmission of digital signals via the current IP/ethernet-based packet-switching networks. However, it lacks backward compatibility and requires huge modifications to the current transport infrastructures. In addition, the current 4G/5G fronthaul is mainly a hub-and-spoke topology with a large number of spoke devices (RUs) connected to a single hub node (DU). However, the optical technology that underpins these networks is still based on fixed point-to-point (PtP) connections which leads to high capital expenditure (CapEx) and operational expenditure (OpEx) [1].

To effectively overcome these technical challenges, the 5G Infrastructure Public Private Partnership (5G-PPP) project, 5G X-haul, proposes a seamlessly converged PtMP wireless-optical transport network solution with a unified software-defined networking (SDN)-based control plane to jointly integrate backhaul and 4G/5G fronthaul services. 5G X-haul aims to offer a flexible allocation of network resources for both fixed and mobile end-users to minimize network CapEx and OpEx [4]. Similarly, the European H2020 5G-Crosshaul project is also targeting the integration of existing and new fronthaul and backhaul technologies and interfaces using point-to-multipoint network topologies [5].

Reconfigurable optical add/drop multiplexers (ROADMs) are regarded as one of the most vital networking elements in the practical realization of future PtMP 5G X-haul and 5G Crosshaul network architectures [6], [7]. The deployment of ROADMs in 5G fronthauls allows the seamless transformation of the current PtP DU-RU links into a reconfigurable PtMP infrastructure with reduced hardware and improved gains due to the statistical multiplexing of user traffic [8]. In addition, ROADMs have demonstrated excellent efficiency to enable network reconfigurability capabilities in metro/access networks [9], thus recent years have seen numerous advanced ROADM architectures proposed to achieve color-less, direction-less, and contention-less ROADMs (CDC-ROADMs) [10]. In addition, low-loss, cost-effective, small-scale, integrated photonic ROADMs have also been introduced [9], [11]–[13] to enable flexible network reconfigurations in high-capacity 5G fronthauls. However, all those ROADMs including the currently commercially available ROADMs are only capable of providing switching functionality at the wavelength level, this constrains the flexibility, dynamic adaptability, latency reduction and cost-effectiveness of future 5G networks where a finer optical switching granularity is highly desirable.

Digital signal processing (DSP)-based, software-reconfigurable, digital filter enabled [14], O-E-O conversion- and optical filter-free, SDN-controllable ROADMs, termed soft-ROADMs, have been recently proposed and experimentally demonstrated to offer increased network flexibility and fine granularity and dynamic reconfigurability in access/metro networks. The soft-ROADMs achieve flexible optical switching at wavelength, sub-wavelength (SW) and spectrally-overlapped orthogonal (I and Q) sub-band (SB)

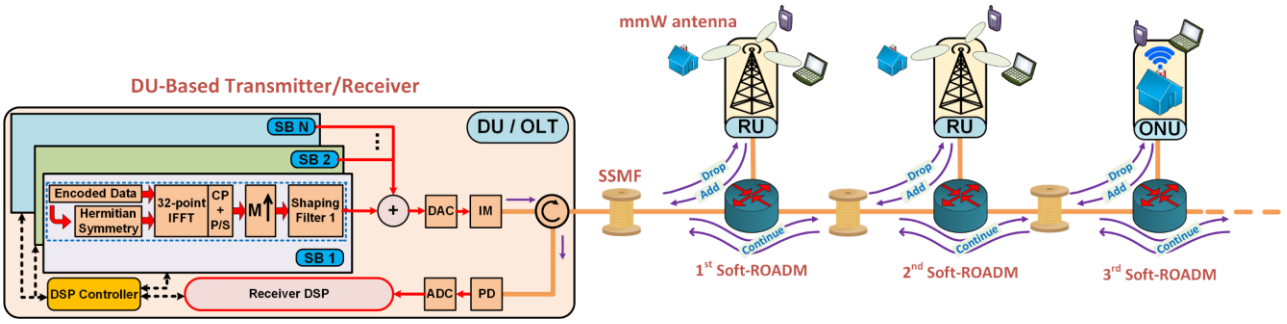

Fig. 1. Schematic diagram of the PtMP 5G fronthaul incorporating soft-ROADMs. SB: sub-band, CP: cyclic prefix, P/S: parallel-to-serial conversion, DAC: digital-to-analogue converter, IM: intensity modulator, ONU: optical network unit, OLT: optical line terminal, DU: distributed unit, RU: radio unit, IFFT: inverse fast Fourier transform, SSMF: standard single-mode fiber.

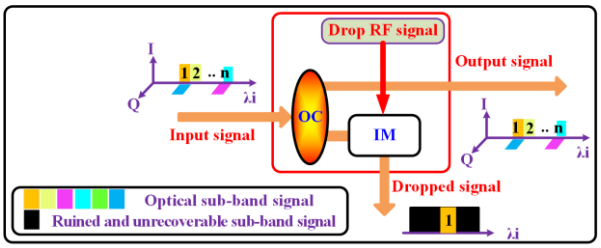

Fig. 2. Soft-ROADM drop element. SB: sub-band, TSB: targeted sub-band.

levels. In addition, soft-ROADMs achieve a great relaxation of the receiver sampling speed requirement as the receiver only needs to support the maximum bandwidth of the dropped SB. The soft-ROADMs' performance has been comprehensively investigated and verified both numerically and experimentally [15], [16]. The low cost and flexibility of the soft-ROADMs also makes them ideally suited to overcome the aforementioned challenges of 5G fronthauls.

To optically drop a targeted sub-band (TSB) signal, the soft-ROADM employs a simple intensity modulation operation on the input optical signal in an optical intensity modulator (IM) driven by an RF local oscillator (LO)-generated sinusoidal drop RF signal, which has the same phase and frequency as the TSB. However, as experimentally observed in [15], the achievable performance of the dropped TSB is highly sensitive to drop RF signal phase offset as any deviation from the optimum phase results in intra-SB attenuation of the dropped TSB and inter-SB leakage between spectrally overlapped orthogonal I and Q SBs. Accurately controlling the drop RF signal's phase provides a significant technical challenge, hindering the practical deployment of soft-ROADMs for cost-sensitive future converged 5G networks as mitigating the impact of drop RF signal phase offset using feedback-based phase control is not a practical solution.

To address the abovementioned technical challenge, this paper presents a novel dual-arm drop element with a Multi-Input Multi-Output (MIMO)-based I/Q crosstalk mitigation technique to eliminate the soft-ROADM drop RF signal phase offset effects. Compared with the conventional detection technique in [15], the newly proposed soft-ROADM with a DSP-implemented, MIMO-based I/Q crosstalk mitigation technique achieves LO phase-insensitive performance, as such the soft-ROADM drop performance is insensitive to any arbitrary drop RF signal phase. It is also shown that the new technique mitigates any intra-SB attenuation and inter-SB leakage effects induced as a result of the fiber's chromatic dispersion experienced by the targeted optical signal. Thus, it significantly simplifies the practical implementation of the soft-ROADMs for future converged 5G networks.

II. Principle of Soft-ROADMs Drop Function

Fig. 1 illustrates the schematic diagram of the soft-ROADM-based PtMP 5G fronthaul architecture where a single DU-located high-speed, IMDD-based transceiver utilising DSP-enabled digital filter multiplexing [14], [15], is used to simultaneously receive/send independent signals from/to multiple concurrent low-speed receivers at different soft-ROADM/RU locations. In addition, Fig. 1 demonstrates the possibility of integrating both 5G mobile fronthauls and fixed access in a converged mobile-fixed optical access network.

As can be seen in Fig. 1, by making use of digital filtering, the optical signal generated by the DU consists of multiple SBs at different SW-bands. Each SW-band has two digital filtering-enabled spectrally overlapped orthogonal I and Q SBs. To drop a TSB within a specific wavelength in the drop element, the incoming optical signal is firstly split into two portions: the first portion is directly delivered to the passive coupler-based add function, whereas, the second portion passes to a drop element based on an optical IM as illustrated in Fig. 2. By driving the DC-biased IM with a drop RF signal which matches the TSB signal in both frequency and phase, the TSB is shifted to the baseband region with a reversed spectrum at the output of the IM, while all other non-targeted SBs (n-TSBs) of the same wavelength are ruined and unrecoverable. At a single-I/Q detection-based drop element, a simple analogue baseband filter is employed after the direct detection photodetector and before the analogue-to-digital converter to separate the TSB from the ruined SBs. Thus, the drop operation offers a significant relaxation of the required bandwidth and completely eliminates the need for further digital matching filtering.

III. The Effect of Drop RF Signal Phase Offset

To simplify the theoretical analysis, ideal digital filter responses and IMs are assumed. In the DU-based transmitter, the generated, real-valued electrical signals for I and Q SBs occupying the i^{th} SW-band can be approximated as:

$$S_i^I(t) = a_i^I(t)\cos\left(2\pi f_{c_i} t\right) \quad (1)$$

$$S_i^Q(t) = a_i^Q(t)\sin\left(2\pi f_{c_i} t\right) \quad (2)$$

where $a_i^I(t)$ and $a_i^Q(t)$ are the double-sideband (reversed-spectrum) I and Q SB data signals of the i^{th} SW-band respectively, f_{c_i} is the central frequency of the digital filter:

$$f_{c_i} = [2 \times i - 1] \times f_{dac}/(2M) \quad (3)$$

where f_{dac} is the digital-to-analogue converter (DAC) sampling frequency in the receiver side, and M is the digital filter up-sampling factor. The total transmitter side optimum

DC-biased, real-valued electrical signal containing the u SW-bands is:

$$S_{elec}^{Total}(t) = \left[\sum_{i=1}^{u}\sum_{w=\{I,Q\}} S_i^w(t)\right] + v \quad (4)$$

where v is the optimum DC bias current. For a specific optical carrier frequency, f_o, the total transmitted optical signal containing u SW-bands after an ideal IM operation can be expressed as:

$$S_{opt}^{Total}(t) = \sqrt{S_{elec}^{Total}(t)}e^{j2\pi f_o t} \quad (5)$$

For the soft-ROADM drop operation, the optimum DC-biased drop RF signals for I and Q drop elements are:

$$S_{RF_i}^I(t) = \cos\left(2\pi f_{c_i} t + \theta_{RF_i}\right) + v_{RF_i}^I \quad (6)$$

$$S_{RF_i}^Q(t) = \sin\left(2\pi f_{c_i} t + \theta_{RF_i}\right) + v_{RF_i}^Q \quad (7)$$

where $v_{RF_i}^I$ ($v_{RF_i}^Q$) represent the optimum DC bias current for I(Q) drop element of the i^{th} SW-band, and θ_{RF_i} is the drop RF signal phase offset relative to the ideal phase.

The optical signal at the output of the soft-ROADM IM can be described as:

$$S_{opt-dropped_i}^w(t) = \sqrt{S_{RF_i}^w(t)S_{opt}^{Total}(t)}, \quad (w = I, Q) \quad (8)$$

For simplicity, we only consider the theoretical analysis for the drop RF signal and the optical signals of the same i^{th} SW-band since the mixing between the i^{th} drop RF signal and the other n-TSBs results in ruined and unrecoverable signal bands that are removed by filtering, therefore:

$$S_{opt-dropped_i}^I(t) = \sqrt{S_{RF_i}^I(t)S_i^I(t) + S_{RF_i}^I(t)S_i^Q(t)}\, e^{j2\pi f_o t} \quad (9)$$

$$S_{opt-dropped_i}^Q(t) = \sqrt{S_{RF_i}^Q(t)S_i^I(t) + S_{RF_i}^Q(t)S_i^Q(t)}\, e^{j2\pi f_o t} \quad (10)$$

After direct detection in the single-I/Q receiver, ignoring noise effects, the resultant dropped electrical signals for I and Q SBs in the i^{th} SW-band are represented as:

$$S_{elec-dropped_i}^I(t) = \beta_i^I\left[S_{RF_i}^I(t)S_i^I(t) + S_{RF_i}^I(t)S_i^Q(t)\right] \quad (11)$$

$$S_{elec-dropped_i}^Q(t) = \beta_i^Q\left[S_{RF_i}^Q(t)S_i^I(t) + S_{RF_i}^Q(t)S_i^Q(t)\right] \quad (12)$$

where β_i^I and β_i^Q take into account all signal losses during the signal recovery process. The terms $S_{RF_i}^I(t)S_i^I(t)$ and $S_{RF_i}^Q(t)S_i^Q(t)$ are the desired I and Q SBs respectively, whereas the terms $S_{RF_i}^I(t)S_i^Q(t)$ and $S_{RF_i}^Q(t)S_i^I(t)$ denote inter-sub-band leakage components between the I and Q SBs in the i^{th} SW-band.

After suitable low-pass filtering, the electrical baseband dropped TSBs in (11) and (12) are expressed as:

$$S_{elec-dropped_i}^I(t) = \beta_i^I\left[a_i^I(t)\cos\left(\theta_{RF_i}\right) - a_i^Q(t)\sin\left(\theta_{RF_i}\right)\right] \quad (13)$$

$$S_{elec-dropped_i}^Q(t) = \beta_i^Q\left[a_i^I(t)\sin\left(\theta_{RF_i}\right) + a_i^Q(t)\cos\left(\theta_{RF_i}\right)\right] \quad (14)$$

Equations (13) and (14) show the drop RF signal phase offset θ_{RF_i} causes an amplitude variation of the dropped TSB which is proportional to $\cos(\theta_{RF_i})$ and inter-SB leakage proportional to $\sin(\theta_{RF_i})$. In addition, all low and high-frequency SBs are equally affected by θ_{RF_i}, and that all frequency components within a SB are also equally affected.

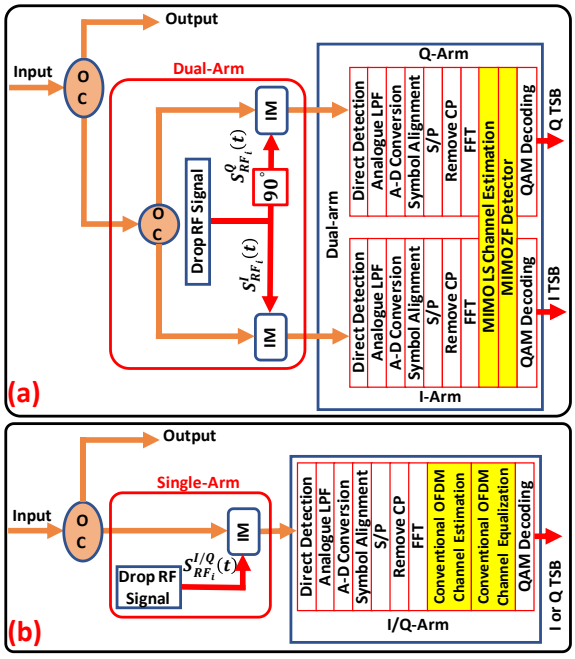

Fig. 3. Soft-ROADM drop elements, (a) dual-arm IQ drop element with MIMO-based I/Q crosstalk mitigation, (b) single-arm I/Q drop element. OC: optical coupler, CP: OFDM cyclic prefix, FFT: fast Fourier transform.

IV. MIMO-BASED I/Q CROSSTALK MITIGATION TECHNIQUE

Equations (13) and (14) show that, when $\theta_{RF_i} \neq 0$, the dropped TSB with single-I/Q detection is a linear combination of both orthogonal I and Q SBs. Based on this fact, we propose a new soft-ROADM-based dual-arm drop element and a novel MIMO-based I/Q crosstalk mitigation technique as shown in Fig. 3(a), for comparison the single-arm I/Q soft-ROADM drop element is shown in Fig. 3(b). To realize the proposed MIMO-based I/Q crosstalk mitigation approach, a dual-arm drop element and a dual input IQ receiver are deployed to achieve a linear 2×2 MIMO system where data-aided MIMO least squares (LS) channel estimation and MIMO zero-forcing (ZF) detection are employed for IQ demultiplexing. A single RF LO and a 90° phase shifter are employed in the dual-arm drop element to achieve suitable orthogonal I and Q drop RF signals required to drive two IMs to produce the optical signals defined in (9) and (10) at the output of the IMs. The proposed MIMO-based I/Q crosstalk mitigation can recover both I and Q SBs in the same SW-band at the same time, whereas two independent single-I/Q receivers would be required to recover both I and Q SBs.

Considering the orthogonal frequency division multiplexing (OFDM) modulation technique, after a fast Fourier transform (FFT) operation, for any OFDM subcarrier k, the two received frequency domain signals from both arms of the dual-arm IQ drop element can be expressed as:

$$y_{k,i}^I = h_{k,i}^{II}x_{k,i}^I + h_{k,i}^{IQ}x_{k,i}^Q + w_{k,i}^I \quad (15)$$

$$y_{k,i}^Q = h_{k,i}^{QI}x_{k,i}^I + h_{k,i}^{QQ}x_{k,i}^Q + w_{k,i}^Q \quad (16)$$

where $y_{k,i}^I$ ($x_{k,i}^I$) and $y_{k,i}^Q$ ($x_{k,i}^Q$) are the received (transmitted) frequency-domain encoded data conveyed on the k^{th} subcarrier of I and Q SBs in the i^{th} SW-band respectively. $h_{k,i}^{II}$ and $h_{k,i}^{QQ}$ are the intra-sub-band coefficients, and $h_{k,i}^{IQ}$ and

$h_{k,i}^{QI}$ are the inter-sub-band coefficients. $w_{k,i}^{I}$ and $w_{k,i}^{Q}$ represent noise. The traditional single-arm I/Q drop element assumes that, after the FFT operation, for any OFDM subcarrier k, the received frequency domain signal is:

$$y_{k,i}^{w} = h_{k,i}^{ww} x_{k,i}^{w} + w_{k,i}^{w}, \quad (w = I \text{ or } Q) \tag{17}$$

For the proposed MIMO-based I/Q crosstalk mitigation, (15) and (16) can be regarded as a system of linear equations, thus they can be expressed in a matrix form as:

$$\begin{bmatrix} y_{k,i}^{I} \\ y_{k,i}^{Q} \end{bmatrix} = \begin{bmatrix} h_{k,i}^{II} & h_{k,i}^{IQ} \\ h_{k,i}^{QI} & h_{k,i}^{QQ} \end{bmatrix} \begin{bmatrix} x_{k,i}^{I} \\ x_{k,i}^{Q} \end{bmatrix} + \begin{bmatrix} w_{k,i}^{I} \\ w_{k,i}^{Q} \end{bmatrix} \tag{18}$$

which is:

$$y_{k,i} = H_{k,i} x_{k,i} + w_{k,i} \tag{19}$$

where $y_{k,i}$ is the 2×1 vector of received encoded data conveyed on the k^{th} subcarrier of the i^{th} SW-band, $x_{k,i}$ is the 2×1 transmitted signal vector, $H_{k,i}$ the is 2×2 MIMO sub-band coefficients matrix, and $w_{k,i}$ is the 2×1 noise vector.

To estimate the MIMO sub-band coefficients matrix, we consider a set of J training symbols $p_{1_{k,i}}, \ldots, p_{J_{k,i}}$. The corresponding received signals can be expressed as:

$$Y_{k,i} = H_{k,i} P_{k,i} + W_{k,i} \tag{20}$$

where $P_{k,i} = [p_{1_{k,i}}, \ldots, p_{J_{k,i}}]$ is the $2 \times J$ training symbol matrix, $Y_{k,i} = [y_{1_{k,i}}, \ldots, y_{J_{k,i}}]$ is the $2 \times J$ matrix of received signals, and $W_{k,i} = [w_{1_{k,i}}, \ldots, w_{J_{k,i}}]$ is the $2 \times J$ noise matrix. $p_{m_{k,i}}$, $y_{m_{k,i}}$, and $w_{m_{k,i}}$ are all 2×1 vectors where $m = 1,2, \ldots, J$. An estimate of $H_{k,i}$ can be now estimated using the LS approach [17], where:

$$\hat{H}_{k,i_{LS}} = Y_{k,i} P_{k,i}^{\dagger} \tag{21}$$

where $P_{k,i}^{\dagger} = P_{k,i}^{H} \left(P_{k,i} P_{k,i}^{H}\right)^{-1}$ is the pseudo-inverse of $P_{k,i}$. $(.)^{H}$ denotes the Hermitian transpose, and $(.)^{\dagger}$ represents pseudo-inverse operation.

As the sub-band coefficients matrix is now known, the ZF estimate [18] of the transmitted data is expressed as:

$$\hat{x}_{k,i_{ZF}} = \hat{H}_{k,i_{LS}}^{\dagger} y_{k,i} \tag{22}$$

where $\hat{H}_{k,i_{LS}}^{\dagger}$ is the pseudo-inverse of the estimated channel coefficients matrix $\hat{H}_{k,i_{LS}}$.

V. NUMERICAL SETUP

The key system parameters are listed in Table I. The Hilbert-pair approach [14] is adopted to construct three digital filter pairs with zero excess of bandwidth and a filter length of $L = 32$. The central frequencies of the digital filter pairs satisfy (3) with $i = 2,3,4$. Similar to [16], in the DU-based transmitter, six real-valued digitally combined OFDM (3-I and 3-Q) SBs are employed in 3 SW-bands as shown in Fig. 4, where the baseband frequency region is kept free to be occupied with the dropped TSB. For each SB, a real-valued OFDM signal containing 14 16QAM-encoded data-carrying subcarriers is generated at the output of a 32-point inverse fast Fourier transform (IFFT) by adopting Hermitian symmetry at the IFFT input, the resultant signal is then up-sampled by a factor of $M = 8$, and digitally filtered with a Hilbert-pair-based I/Q shaping filter to dynamically locate the SB signal at the desired SW-band [14]. The different SB signals are then digitally combined as shown in Fig. 1. The total signal is then clipped, quantized, and converted into an optical signal using ideal IM after a 8-bit, 15GS/s DAC.

TABLE I: LIST OF PARAMETERS

Parameter	Value
DAC sampling speed	15GS/s
ADC sampling speed	1.875GS/s
Bandwidth of SW-band (before drop operation)	1.875GHz
Bandwidth of SW-band (after drop operation)	937.5MHz
Bandwidth of electrical LPF	937.5MHz
DAC/ADC resolution	8 bits
Clipping ratio	14 dB
OFDM IFFT/FFT size	32
Cyclic prefix	12.5%
Modulation format	16 QAM
Data-carrying subcarriers	14
Up-sampling factor (M)	8
Bit rate per channel	2.92 Gbps
Total bit rate	17.5 Gbps
Digital filter roll-off factor	0
Digital filter length	32
Optical wavelength	1550 nm
APD quantum efficiency	0.8
APD sensitivity	-26 dBm
Total optical launch power	3 dBm

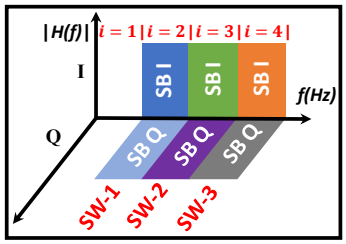

Fig. 4. Spectral locations of six digitally filtered OFDM SBs in 3 SW-band spectral regions SB: sub-band, TSB: targeted sub-band.

To effectively highlight the performance characteristics of the soft-ROADM drop operation, ideal IMs are employed to perform the drop operation. At the single-arm (dual-arm) drop element, an APD(s) with a quantum efficiency of 0.8 and a power sensitivity of -26 dBm are employed for the direct detection followed by a 937.5MHz analogue low-pass filter(s) (LPFs) before 1.875GS/s analogue-to-digital converter(s) (ADCs). Thus, no digital filtering is required.

VI. RESULTS AND DISCUSSIONS

A. *Drop Operation Robustness to Drop RF Signal Phase Offset*

Fig. 5(a) shows the effect of drop RF signal phase offset on the BER of each dropped TSB when only either 3-I or 3-Q SBs are occupied and the total received optical power (T-ROP) is set to -17.2 dBm after the drop operation and before direct detection which corresponds to an optical power of -22 dBm for each individual OFDM SB after the drop operation. The result agrees with (13) and (14) and demonstrates the impact of phase-offset-induced amplitude variations, when the single-arm I/Q drop element is employed, which is the minimum (highest) at $\theta_{RF_i} = 0, \pm m\pi$ where $m = 1,2,3 \ldots (\theta_{RF_i} = \pm n\pi/2$ where $n = 1,3,5 \ldots)$. Similarly, Fig. 5(b) shows the impact of drop RF signal phase offset on the BER of each dropped TSB when all 6 SBs are occupied at a fixed T-ROP of -14.2 dBm (-22 dBm per OFDM SB) after the drop operation. Compared with Fig. 5(a), Fig. 5(b) shows that, when using the single-arm I/Q drop element, drop RF signal

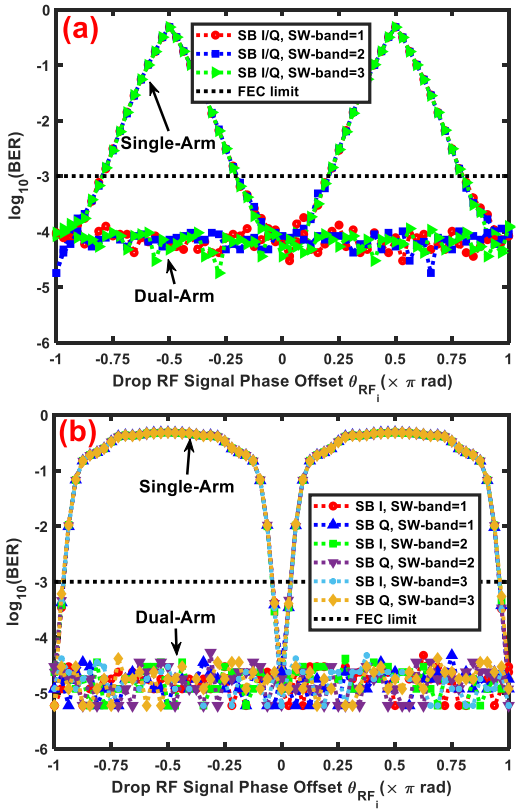

Fig. 5. BER vs. drop RF signal phase offset when (a) only 3-I or 3-Q SBs are occupied, (b) both 3-I and 3-Q SBs are occupied.

phase offset has a higher impact when both I and Q SBs exist together due to the additional effect of phase-offset-induced inter-sub-band leakage as indicated in (13) and (14). The results in Figs. 5(a) and 5(b) demonstrate the ability of the dual-arm IQ drop element to completely mitigate the effect of drop RF signal phase offset in any I/Q SB at any low/high SW-band ensuring a phase-offset-independent SW-band/SB-independent performance. In addition, the result in Fig. 5(a) is clear evidence that the dual-arm IQ drop element does not require both orthogonal I and Q SBs to be occupied to operate.

Equations (13) and (14) suggest that, as the desired (undesired) signal disappears from one arm, due to drop RF signal phase offset, it appears as an undesired (desired) signal at the other arm of the dual-arm IQ drop element without power loss. Depending on θ_{RF_i}, both arms can receive different combinations of I and Q SBs. However, with the MIMO-based I/Q crosstalk mitigation technique, the fact that the resultant BER is independent of θ_{RF_i} validates the efficiency of our proposed technique to mitigate any level of inter-sub-band leakage between the orthogonal I and Q SBs.

B. *Performance/Capacity Trade-off between Orthogonal Sub-bands*

The newly proposed dual-arm IQ drop element can also potentially be employed to intentionally adjust the drop RF signal phase to achieve performance/capacity trade-off between orthogonal SBs when the I and Q arms have different noise/distortion performance. Fig. 6 shows the trade-off relationship at a fixed T-ROP of -14.2dBm after the drop operation, considering a white ADC timing jitter [19] of 8% (2%) unit intervals rms (UI_{rms}) in the I-arm (Q-arm). At $\theta_{RF_i} = 0$, Q-SB shows better BER and higher achievable bit rate whereas I-SB fails to achieve a BER below the adopted

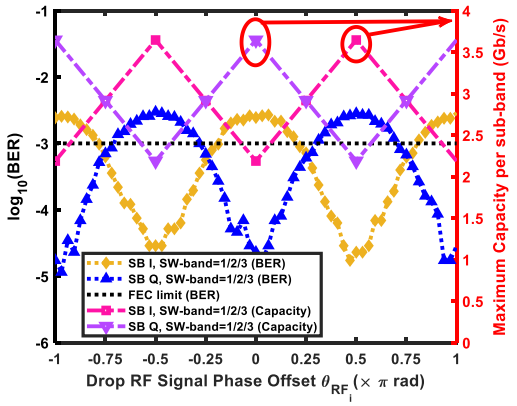

Fig. 6. BER/capacity trade-off relationship using dual-arm IQ drop element.

BER forward error correction (FEC) limit, drop RF signal phase can be adjusted to control the power distribution of I and Q SBs in each arm to either achieve a balance in the BER/capacity at $\theta_{RF_i} = \pm n\pi/4$ or to trade-off the BER/capacity between orthogonal SBs. To obtain the maximum achievable capacity for each SB, adaptive bit-loading is utilized in each subcarrier in each SB where subcarriers modulation formats are selected from 128/64/32/16/8/4-QAM, and DBPSK, the highest possible subcarrier modulation format is chosen while ensuring that the total BER is below the adopted BER FEC limit.

C. *Drop Operation Robustness to Channel Roll-off Effects*

To explore the robustness of the proposed technique to IQ crosstalk-inducing channel roll-off effects, we employ a LPF after the DAC and before E-O conversion in the transmitter in Fig. 1. The inset in Fig. 7(b) shows the characteristics of the employed LPF which is similar to the filter employed in [20]. The employed LPF has a frequency response roll-off of about 5.5 dB within 0-7.25 GHz spectral range.

Fig. 7(a) shows the performance of the proposed dual-arm IQ drop element compared with the single-arm I/Q drop element as the received optical power is varied whilst the drop RF signal phase offset is kept constant at 0 and when the LPF is not employed. The result shows that, under the ideal conditions, both techniques show similar BER developing trends. Whereas, as illustrated in Fig. 7(b), when the LPF is employed in the transmitter, the proposed dual-arm IQ drop element has superior performance as it has excellent ability in mitigating the impact of inter sub-band leakage caused by the channel-induced roll-off effects with an optical power penalty of <0.5dB (at a fixed BER of 1×10^{-3}) when compared with Fig. 7(a). The single-arm I/Q drop element completely fails to achieve a BER below the FEC limit when the LPF is employed which emphasizes the fact that it is not able to mitigate the impact of channel-roll-off-induced I/Q leakage effects.

D. *Drop Operation Robustness to Fiber Transmission Effects*

The impact of fiber chromatic dispersion on receiver sensitivity is illustrated in Fig. 8 where the length of the employed single-mode fiber (SMF) is varied, the SMF has a dispersion parameter (dispersion slope) of 16 ps/nm/km (0.08 ps/nm^2/km). Receiver sensitivity indicates the minimum required ROP to achieve a BER at the adopted FEC limit. It can be seen in Fig. 8 that the SBs that occupy the 1st SW-band are virtually unaffected by fiber chromatic dispersion. In addition, SBs occupying the 2nd SW-band are less affected

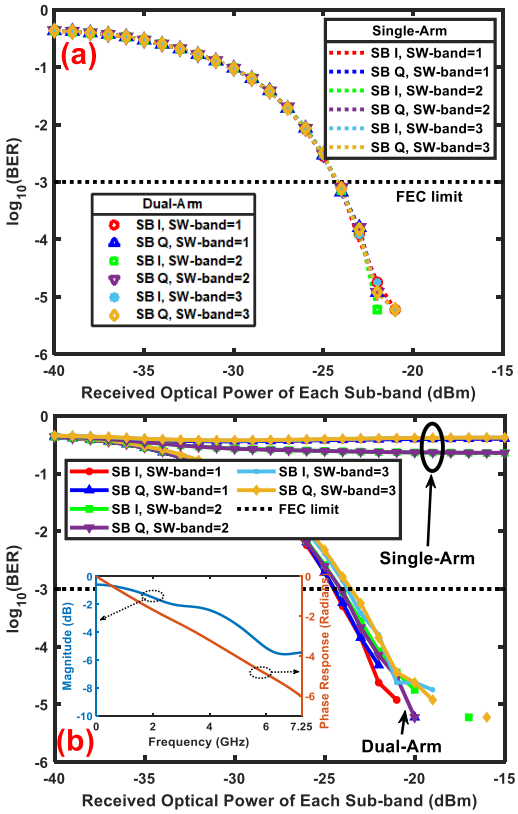

Fig. 7. BER performances of soft-ROADM drop operation; (a) optical back-to-back connection, (b) with a LPF at the DU-based transmitter. The inset shows the characteristics of the LPF employed at the DU-based transmitter to introduce roll-off effect.

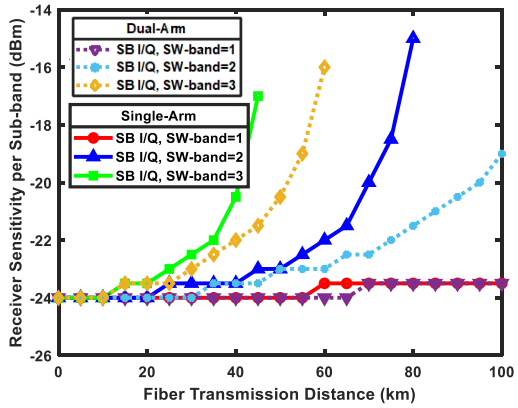

Fig. 8. Drop operation performance robustness to fiber chromatic dispersion.

than the SBs occupying the 3rd SW-band. However, the dual-arm IQ drop element clearly offers more robustness against fiber chromatic dispersion and offers better receiver sensitivity with a lower fiber-induced optical power penalty.

VII. CONCLUSION

A new dual-arm IQ drop element-based soft-ROADM incorporating a novel MIMO-based I/Q crosstalk mitigation technique is demonstrated for application in flexible PtMP 5G fronthaul, the new soft-ROADM eliminates the need to dynamically control the drop RF signal phase, and increases the robustness to fiber chromatic dispersion and channel roll-off effects, thus making the new soft-ROADM significantly simpler to practically implement for 5G fronthaul. Experimental demonstration of the technique is currently in progress.

ACKNOWLEDGMENT

This work was supported by the DSP Centre of Excellence funded by the European Regional Development Fund (ERDF) through the Welsh Government.

REFERENCES

[1] Y. Fan *et al.*, "Point-to-Multipoint Coherent Architecture with Joint Resource Allocation for B5G/6G Fronthaul," *IEEE Wirel. Commun.*, vol. 29, no. 2, pp. 100–106, Apr. 2022.

[2] J. Bartelt *et al.*, "5G transport network requirements for the next generation fronthaul interface," *EURASIP J. Wirel. Commun. Netw.*, vol. 2017, no. 1, p. 89, Dec. 2017.

[3] X. Liu, *Optical communications in the 5G era*. London: Academic Press, 2022.

[4] D. Camps-Mur *et al.*, "5G-XHaul: A Novel Wireless-Optical SDN Transport Network to Support Joint 5G Backhaul and Fronthaul Services," *IEEE Commun. Mag.*, vol. 57, no. 7, pp. 99–105, Jul. 2019.

[5] X. Costa-Perez *et al.*, "5G-Crosshaul: An SDN/NFV Integrated Fronthaul/Backhaul Transport Network Architecture," *IEEE Wirel. Commun.*, vol. 24, no. 1, pp. 38–45, Feb. 2017.

[6] C. Vagionas *et al.*, "End-to-End Real-Time Service Provisioning Over a SDN-Controllable Analog mmWave Fiber -Wireless 5G X-Haul Network," *J. Lightw. Technol.*, vol. 41, no. 4, pp. 1104–1113, Feb. 2023.

[7] J. Yu, S. Zhu, and K. Daniel, "Evolution to Mesh 5G X-Haul Networks," in *2020 Optical Fiber Communications Conference and Exhibition (OFC)*, San Diego, CA, US, 2020, pp. 1–3.

[8] G. Kalfas *et al.*, "Next Generation Fiber-Wireless Fronthaul for 5G mmWave Networks," *IEEE Commun. Mag.*, vol. 57, no. 3, pp. 138–144, Mar. 2019.

[9] E. Ruggeri *et al.*, "Reconfigurable Fiber Wireless Fronthaul With A-RoF and D-RoF Co-Existence Through a Si3N4 ROADM for Heterogeneous Mmwave 5G C-RANs," *J. Lightw. Technol.*, vol. 40, no. 16, pp. 5514–5521, Aug. 2022.

[10] Y. Li, J. Lin, L. Zong, S. K. Bose, B. Mukherjee, and G. Shen, "Colorless, partially directionless, and contentionless architecture for high-degree ROADMs," *J. Opt. Commun. Netw.*, vol. 14, no. 6, pp. 481–492, Jun. 2022.

[11] C. Browning *et al.*, "A Silicon Photonic Switching Platform for Flexible Converged Centralized-Radio Access Networking," *J. Lightw. Technol.*, vol. 38, no. 19, pp. 5386–5392, Oct. 2020.

[12] A. Tsakyridis *et al.*, "Reconfigurable Fiber Wireless IFoF Fronthaul With 60 GHz Phased Array Antenna and Silicon Photonic ROADM for 5G mmWave C-RANs," *IEEE J. Sel. Areas Commun.*, vol. 39, no. 9, pp. 2816–2826, Sep. 2021.

[13] C. Mitsolidou *et al.*, "A 5G C-RAN Optical Fronthaul Architecture for Hotspot Areas Using OFDM-Based Analog IFoF Waveforms," *Appl. Sci.*, vol. 9, no. 19, p. 4059, Sep. 2019.

[14] M. Bolea, R. P. Giddings, M. Bouich, C. Aupetit-Berthelemot, and J. M. Tang, "Digital filter multiple access PONs with DSP-enabled software reconfigurability," *J. Opt. Commun. Netw.*, vol. 7, no. 4, pp. 215–222, Apr. 2015.

[15] E. Al-Rawachy, R. P. Giddings, and J. M. Tang, "Real-time experimental demonstration of DSP-enabled soft-ROADMs with multi-level flexible add/drop functions for cloud access networks," *Opt. Express*, vol. 27, no. 1, pp. 16–33, Jan. 2019.

[16] W. Jin *et al.*, "Improved Performance Robustness of DSP-Enabled Flexible ROADMs Free from Optical Filters and O-E-O Conversions," *J. Opt. Commun. Netw.*, vol. 8, no. 8, pp. 521–529, Aug. 2016.

[17] M. Biguesh and A. B. Gershman, "Training-based MIMO channel estimation: a study of estimator tradeoffs and optimal training signals," *IEEE Trans. Signal Process.*, vol. 54, no. 3, pp. 884–893, Mar. 2006.

[18] C. Wang, E. Au, R. Murch, W. Mow, R. Cheng, and V. Lau, "On the Performance of the MIMO Zero-Forcing Receiver in the Presence of Channel Estimation Error," *IEEE Trans. Wirel. Commun.*, vol. 6, no. 3, pp. 805–810, Mar. 2007.

[19] O. F. A. Gonem, R. P. Giddings, and J. Tang, "Timing Jitter Analysis and Mitigation in Hybrid OFDM-DFMA PONs," *IEEE Photonics J.*, vol. 13, no. 6, pp. 1–13, Dec. 2021.

[20] Y. Dong, E. Al-Rawachy, R. P. Giddings, W. Jin, D. Nesset, and J. M. Tang, "Multiple Channel Interference Cancellation of Digital Filter Multiple Access PONs," *J. Lightw. Technol.*, vol. 35, no. 1, pp. 34–44, 2017.